energies

MDPI

Article

Frequency-Adaptive Repetitive Voltage Control for Virtual Synchronous Generator Inverters

Ping Xiong [1,2], Lie Li [1,2], Yu Sun [1,2], Jinrui Tang [3] and Keliang Zhou [3,*]

[1] State Grid Hubei Electric Power Research Institute, Wuhan 430077, China; joey.xiongping@gmail.com (P.X.); jzll0902@outlook.com (L.L.); syeden2000@163.com (Y.S.)
[2] Hubei Key Laboratory of Regional New Power Systems and Rural Energy System Configuration, Wuhan 430077, China
[3] School of New Energy and Electrical Engineering, Wuhan University of Technology, Wuhan 430070, China; tangjinrui@whut.edu.cn
* Correspondence: keliang.zhou@whut.edu.cn

Abstract

Virtual Synchronous Generator (VSG)-based grid-forming inverters are widely employed to provide voltage and frequency support for enhancing power system stability in renewable-rich grids. However, their Point of Common Coupling (PCC) voltage quality deteriorates under harmonic perturbations caused by nonlinear loads, grid voltage distortions, and so on. In this paper, an adaptive repetitive voltage control strategy is proposed for VSG inverters to eliminate harmonic perturbations. The proposed method integrates a frequency-adaptive repetitive controller into the state-feedback voltage control loop to ensure accurate harmonic compensation in the presence of nonlinear loads, grid voltage distortions, and grid frequency variations. A plug-in design preserves the VSG's inherent grid-forming capabilities while avoiding control loop redesign. Experimental results demonstrate that the proposed voltage control strategy can achieve fast, accurate, and robust PCC voltage regulation to offer voltage support and grid frequency support and provide accurate elimination of harmonic distortions under nonlinear rectifier loads, grid voltage distortions, and grid frequency variations.

Keywords: virtual synchronous generator; repetitive control; harmonic suppression

1. Introduction

In traditional power systems, the inertia of the rotor and the damping on the shaft of synchronous generators (SGs) play crucial roles in maintaining the stable operation of the system. With a high proportion of low- or zero-mechanical-inertia power electronic converter-interfaced distributed generators in power systems, insufficient inertia support from SGs can result in the deterioration of power system operation stability [1]. VSG control is widely used to enable inverters in battery energy storage systems or distributed generators to support power system voltage and frequency stability by emulating the inertia and droop characteristics of real SGs [2–7]. VSG control includes outer-loop power control and inner-loop voltage control [8–10]. The outer-loop power control emulates the behavior of a real SG to generate the reference PCC voltages and then contributes to the regulation of PCC voltages and grid frequency via the inner-loop voltage control. So far, various voltage control methods have been developed to enable PCC voltages to rapidly, accurately and robustly track the reference voltages, such as the Synchronous Reference Frame (SRF) PI control, multivariable state control, and so on [8–14]. However,

Check for updates

Academic Editor: Federico Barrero

Received: 26 August 2026
Revised: 25 September 2026
Accepted: 28 September 2026
Published: 13 October 2026

Copyright: © 2026 by the authors. Licensee MDPI, Basel, Switzerland. This article is an open access article distributed under the terms and conditions of the Creative Commons Attribution (CC BY) license.

these voltage controllers can only guarantee accurate regulation of the fundamental line frequency voltage component and fail to ensure good PCC voltage quality under harmonic distortions caused by nonlinear loads, distorted grid voltages, etc. [15].

Based on the Internal Model Principle (IMP) [16], multi-resonant controllers (MRSCs) use resonant controllers to eliminate harmonic distortions of the PCC voltage at the corresponding harmonic frequencies [17–19]. However, the computational burden and synthesis complexity of MRSCs increase with the number of harmonics, particularly high-order harmonics [20]. In contrast, an IMP-based repetitive controller (RC) can eliminate all harmonic distortions below the Nyquist frequency simultaneously [21–23], which consumes much less computational resources and is much easier to synthesize and implement. It should be noted that the frequency generated by the VSG control scheme varies with the output active power of the inverter-interfaced distributed generators [9]. Moreover, frequency variations substantially degrade the tracking/rejection performance of RCs [21–23]. Therefore, a frequency-adaptive RC is needed to reinforce the inner-loop voltage control scheme to always ensure effective rejection of harmonic perturbations.

To address the above issues, a plug-in frequency-adaptive repetitive controller (FARC) scheme is proposed for VSG inverters to eliminate voltage harmonic distortions at the PCC in the presence of nonlinear loads, grid voltage distortions, grid frequency variations, etc. The proposed method integrates an FARC into the state-feedback voltage control loop to ensure accurate harmonic compensation. The plug-in design preserves the VSG's inherent grid-forming capabilities while avoiding control-loop redesign. A simple but effective approach is developed to synthesize the proposed plug-in FARC voltage control scheme. An application case is studied to verify the effectiveness of the proposed voltage control scheme.

2. Plug-In FARC Voltage Control for VSG Inverters

Figure 1 shows a three-phase grid-forming inverter with a nonlinear rectifier load at the PCC that employs a typical VSG control scheme. The VSG control scheme includes an outer-loop power controller and an inner-loop voltage controller. The outer-loop power controller mimics the behavior of a real SG to generate the reference PCC voltage, $v_m\angle\theta_m$, while the inner-loop voltage controller forces the PCC voltage, v_o, to exactly track the reference PCC voltage, $v_m\angle\theta_m$, under various operating conditions [8].

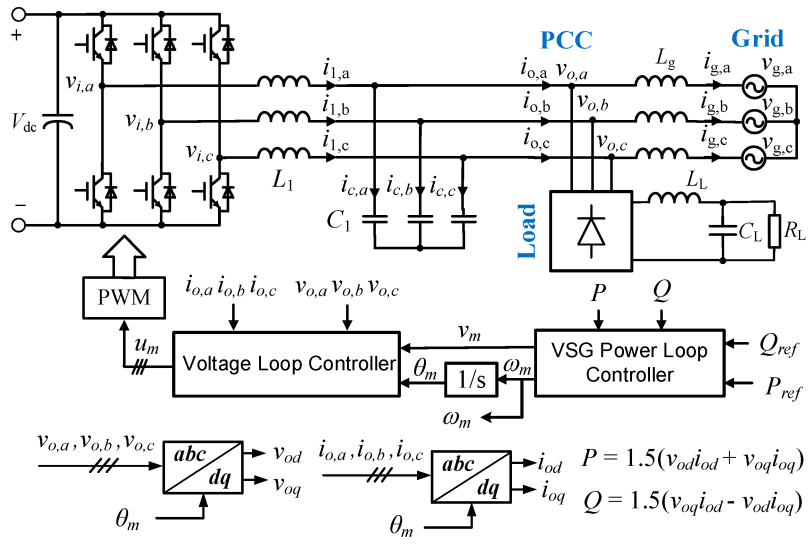


Figure 1. Typical VSG-based three-phase grid-forming inverter.

2.1. VSG Power Controller

The functionalities of the VSG—grid frequency support and droop control—are often defined using the outer-loop power controller, as below [17–19]:

$$J\frac{d\omega_m}{dt} = \frac{1}{\omega_n}(P_{ref} - P) - D(\omega_m - \omega_n) \tag{1}$$

$$v_m = v_o + k_q(Q_{ref} - Q), \tag{2}$$

in which P_{ref} is the reference active power; P is the output active power at the PCC; Q_{ref} is the reference reactive power; Q is the output reactive power at the PCC; J and D are the virtual moment of inertia of the rotor and the damping coefficient of the SGs, respectively; k_q is the voltage regulation coefficient; ω_m is the actual angular frequency; ω_n is the nominal angular frequency of the PCC voltage; and v_m and v_o are the reference PCC voltage and the actual PCC voltage, respectively.

For the outer-loop power controller of VSG inverters, the power controller in (1) is designed to produce the reference phase angle θ_m of the PCC voltage by mimicking the primary frequency response P–ω_m of SGs, while the power controller in (2) is designed to generate the reference PCC voltage by mimicking the droop characteristics Q–v_m of SGs. Briefly speaking, the role of the VSG power-loop controllers in (1) and (2) is to define the grid-forming functionalities of the VSG inverter and generate the reference PCC voltage $v_m\angle\theta_m$.

2.2. Plug-In FARC Voltage Controller

Figure 2 shows the proposed plug-in FARC voltage control scheme for VSG inverters. The proposed voltage control scheme is a complementary combination of a state-feedback controller and a plug-in FARC controller. It aims to make the best use of the complementary capabilities of the two controllers to force the PCC voltages $v_{o,j}$, where the subscript $j = a$, b, and c, to rapidly, accurately, and robustly track the reference voltages, $v_{m,j}$, where the subscript $j = a$, b, and c, under various operating conditions.

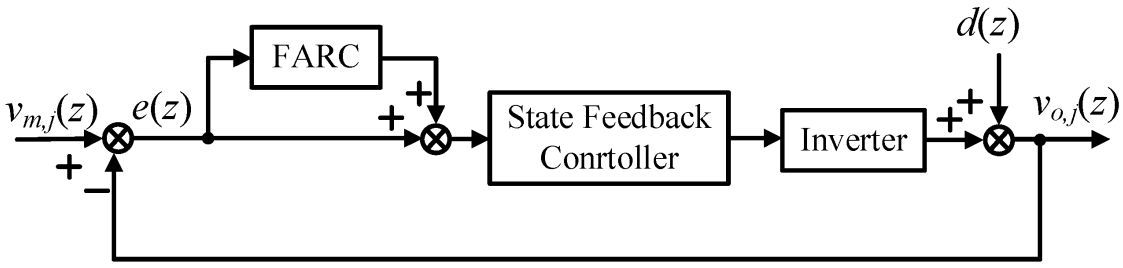


Figure 2. Proposed plug-in FARC voltage control scheme.

The mathematical model of the inverter shown in Figure 1 can be written as follows:

$$\begin{bmatrix} \frac{di_{1,j}(t)}{dt} \\ \frac{dv_{o,j}(t)}{dt} \end{bmatrix} = \begin{bmatrix} 0 & -\frac{1}{L_1} \\ \frac{1}{C_1} & 0 \end{bmatrix} \begin{bmatrix} i_{1,j}(t) \\ v_{o,j}(t) \end{bmatrix} + \begin{bmatrix} \frac{1}{L_1} & 0 \\ 0 & -\frac{1}{C_1} \end{bmatrix} \begin{bmatrix} v_{i,j}(t) \\ i_{o,j}(t) \end{bmatrix}, \tag{3}$$

where $v_{i,j}(t) = \frac{1}{2}V_{dc}u_j(t)$.

The sampled-data model of the inverter in (2) with a sampling interval T_S can be further derived as

$$\begin{cases} X_j(k+1) = \Phi X_j(k) + HU_j(k) \\ Y_j(k) = \Pi X_j(k) \end{cases}, \quad j = a, b, c, \tag{4}$$

where $X_j(k) = \begin{bmatrix} i_{1,j}(k) & v_{o,j}(k) \end{bmatrix}^T$, $U_j(k) = \begin{bmatrix} u_j(k) & i_{o,j}(k) \end{bmatrix}^T$, $\Pi = \begin{bmatrix} 0 & 1 \end{bmatrix}$, $Y_j(k) = v_{o,j}(k)$ $\Phi = \begin{bmatrix} 1 - \frac{T_s^2}{2L_1C_1} & -\frac{T_s}{L_1} \\ \frac{T_s}{C_1} & 1 - \frac{T_s^2}{2L_1C_1} \end{bmatrix}$, and $H = \begin{bmatrix} \frac{V_{dc}T_s}{2L_1} & \frac{T_s^2}{C_1L_1} \\ \frac{V_{dc}T_s^2}{2L_1C_1} & -\frac{T_s}{C_1} \end{bmatrix}$.

According to the inverter model in (4), a state-feedback PCC voltage controller $G_c(z)$ can be developed as [17]

$$U_j(k) = -FX_j(k) + \Psi R_j(k), \quad j = a, b, c, \tag{5}$$

where $R_j(k) = v_{m,j}(k)$; F and Ψ are the controller coefficients.

Substituting (5) into (4), we can get the closed-loop state-feedback control system equation as

$$\begin{cases} X_j(k+1) = (\Phi - HF)X_j(k) + H\Psi R_j(k) \\ Y_j(k) = \Pi X_j(k) \end{cases}. \tag{6}$$

Note that the poles of (6) can be flexibly placed within the unit circle by appropriately choosing F and Ψ. It is well known that F and Ψ can be chosen to yield (Φ − HF) = 0 and HΨ = I. Then, $v_{m,j}$ $(k) = v_{o,j}(k + 1)$, i.e., the deadbeat (DB) response $G_H(z) = v_{o,j}(z)/v_{m,j}(z) = z^{-1}$ is achieved. It can be derived that

$$u_j(k) = -f_{11}i_{1,j}(k) - f_{12}v_{o,j}(k) + \varphi_2 v_{ref,j}(k), \tag{7}$$

where $f_{11} = 2L_1/(V_{dc}T_s)$, $f_{12} = \left(2L_1C_1 - T_s^2\right)/\left(V_{dc}T_s^2\right)$, and $\varphi_2 = 2L_1C_1/\left(V_{dc}T_s^2\right)$.

Since (Φ − HF) = 0, i.e., all poles of (6) are placed at the origin and are therefore far away from the unit circle, the DB system has large stability margins. It is well known that the state-feedback controller cannot ensure accurate regulation of the line-frequency sinusoidal voltage at the PCC under parameter/load uncertainties. A static abc-coordinate resonant controller, such as a PR controller [18] and so on [20], is usually added to the state-feedback controller. However, it cannot achieve accurate compensation of harmonic distortions in the presence of nonlinear loads, grid voltage distortion, etc. Multiple resonant controllers can be used to eliminate harmonic distortions of the PCC voltage at the cost of heavy computational burden and synthesis complexity.

Fortunately, the IMP-based RC can eliminate all harmonic distortions with low computational burden, easy synthesis, etc. Hence, to suppress voltage harmonic distortions at the PCC, an RC controller $G_{rc}(z)$ is plugged into the state-feedback control loop as [22]

$$G_{rc}(z) = \frac{k_{rc}Q(z)z^{-N}}{1 - Q(z)z^{-N}}G_f(z), \tag{8}$$

where $k_{rc} > 0$ denotes the repetitive control gain; $N = f_s/f_m$, where f_s and $f_m = \omega_m/(2\pi)$ are the sampling frequency and reference frequency, respectively; $Q(z) = a_1z + a_0 + a_1z^{-1}$ is usually a low-pass filter with $2a_1 + a_0 = 1$; and $G_f(z)$ is used to compensate for the delay in the state-feedback control system.

Without the plug-in RC $G_{rc}(z)$, the transfer function of the state-feedback-control system shown in Figure 2 can be written as

$$G_H(z) = \frac{G_C(z)G_P(z)}{1 + G_C(z)G_P(z)}. \tag{9}$$

Without loss of generality, $G_H(z)$ in (9) can be expressed as

$$G_H(z) = \frac{L(z)}{M(z)} = \frac{z^{-d}L^+(z)L^-(z)}{M(z)}, \tag{10}$$

where d denotes the number of system delay steps; all roots of $M(z) = 0$ are within the unit circle; $L^-(z)$ includes the zeros of $L(z)$ on or outside the unit circle; and $L^+(z)$ comprises the zeros of $L(z)$ that are not included in $L^-(z)$.

To achieve zero-phase system-delay compensation, $G_f(z)$ for the plug-in RC in (8) can be chosen as [17]

$$G_f(z) = \frac{z^d M(z) L^-(z^{-1})}{L^+(z) p}, \tag{11}$$

where $p \geq \max |\, L^-(z) \,|^2$.

Under the above premise, when the control gain satisfies [17]

$$0 < k_{rc} < 2, \tag{12}$$

the overall control system is asymptotically stable. The larger the gain k_{rc}, the faster the dynamic response of the RC controller. Note that, with a given $G_f(z)$ in (11), the design of the RC in (8) is greatly simplified.

It should be noted that the reference frequency f_m varies with the grid frequency f for VSG inverters [8]. Moreover, variations in f_m can substantially degrade the tracking/rejection performance of the RC [16,17]. As we all know, the RC in (9) with an integer-order N can well eliminate all harmonic perturbations within the bandwidth of $Q(z)$. However, N often becomes fractional when f_m varies, and the fractional delay $z^{-N} = z^{-Ni-D}$, where N_i and D are the integer part and the fractional part of N, respectively, cannot be implemented in practice. The fractional delay z^{-D} can be approximated using an integer-order Fractional-Delay (FD) filter as [17,18]

$$z^{-D} = \sum_{k=0}^{n} A_k z^{-k}, \tag{13}$$

where $0 \leq D < 1$, and the coefficients A_k can be calculated online using Lagrange interpolation as follows:

$$A_k = \prod_{i=0, i \neq k}^{n} \frac{D - i}{k - i}. \tag{14}$$

Note that the FD filter with a larger order n can better approximate the fractional delay z^{-D}, but with high computational complexity [17,18].

Combining (8) and (13), an FARC controller can be formulated as

$$G_{rc,j}(z) = \frac{k_{rc} Q(z) z^{-N_i} z^{-D}}{1 - Q(z) z^{-N_i} z^{-D}} G_f(z). \tag{15}$$

It should be noted that when $N = f_s/f_m$ is an integer, the FARC in (15) becomes the same as the RC in (8).

3. Experimental Results

A 2.5 kVA hardware-in-the-loop grid-connected inverter experimental platform, shown in Figure 3, is built to test the proposed control scheme, whose system parameters are listed in Table 1.

Table 1. System parameters.

Parameters	Value (Unit)
DC-link voltage V_{dc}	400 V
Filter inductor L_1	3.4 mH

Table 1. *Cont.*

Parameters	Value (Unit)
Filter capacitor C_1	10 μF
Sampling frequency f_s	20 kHz
Grid voltage v_g	110 V(RMS)
Nominal angular frequency ω_n	$50 \times 2\pi$ (rad/s)
Line inductor L_g	18 mH
Moment of Inertia of the rotor J	0.09 kg·m^2
Damping coefficient D	1.5
Reference angular frequency ω_n	100π rad/s
Voltage regulation coefficient k_q	0.015
Nominal PCC voltage v_0	110 V(RMS)

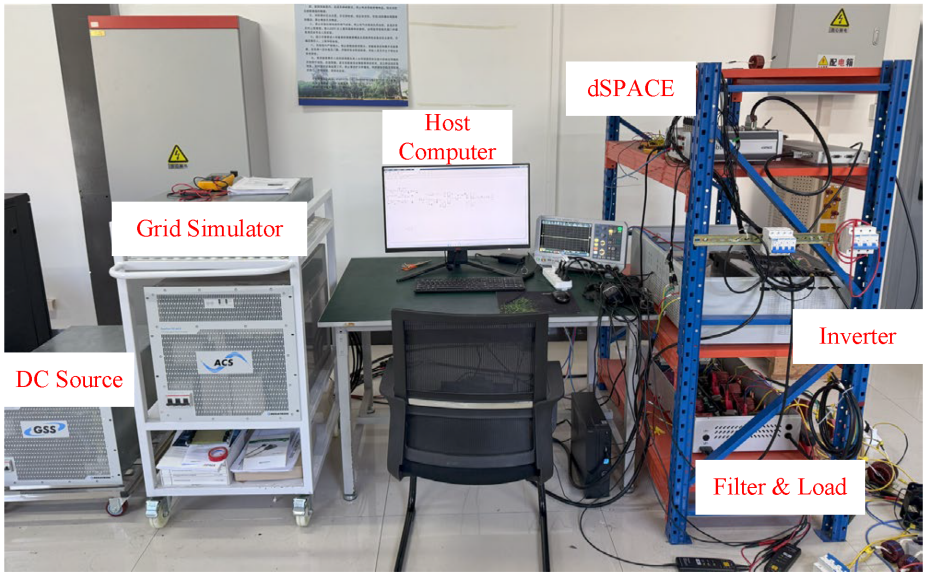


Figure 3. Experimental platform.

Following the proposed method, as shown in Figure 2, an FARC voltage controller $G_{\mathrm{rc}}(z)$ is plugged into the state-feedback controller as follows:

$$\begin{cases} u_j(k) = -f_{11} i_{1,j}(k) - f_{12} v_{o,j}(k) + \varphi_2 v_{m,j}(k) \\ G_{rc}(z) = \frac{k_{rc} Q(z) z^{-N_i} z^{-F}}{1 - Q(z) z^{-N_i} z^{-F}} G_f(z) \end{cases} \quad j = a, b, c,$$

where $f_{11} = 0.34$, $f_{12} = 0.066$, and $\varphi_2 = -0.2$ are the coefficients; $k_{rc} = 0.3$; and $G_f(z) = z$.

For comparison, a plug-in resonant voltage controller $G_r(z)$ [20] is used instead of the FARC voltage controller as follows:

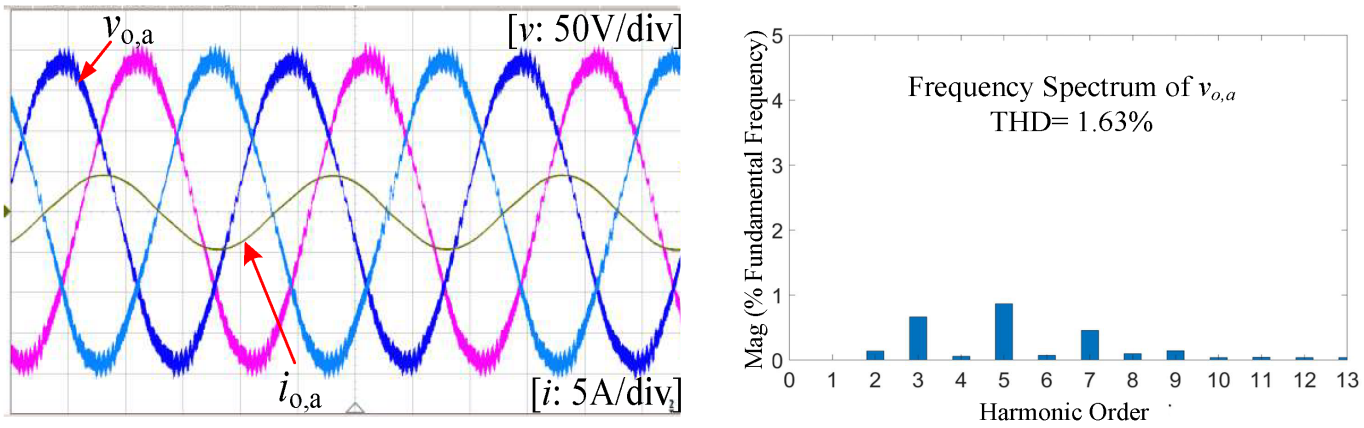
$$\begin{cases} u_j(k) = -f_{11} i_{1,j}(k) - f_{12} v_{o,j}(k) + \varphi_2 v_{m,j}(k) \\ G_r(z) = k_r \frac{\cos(\omega_m T_s + \theta) z^{-1} - z^{-2} \cos(\theta)}{1 - 2\cos(\omega_m T_s) z^{-1} + z^{-2}} G_f(z) \end{cases} \quad j = a, b, c,$$

where $k_r = 0.6$ is the resonant control gain; and $\theta = 0$ is the phase-lead angle employed to compensate for unmodelled delays.

3.1. System Responses Without Harmonic Perturbations

In this case, the rectifier load is not connected to the PCC, the grid voltage v_g is free of harmonic distortions, and the grid frequency $f = 50$ Hz.

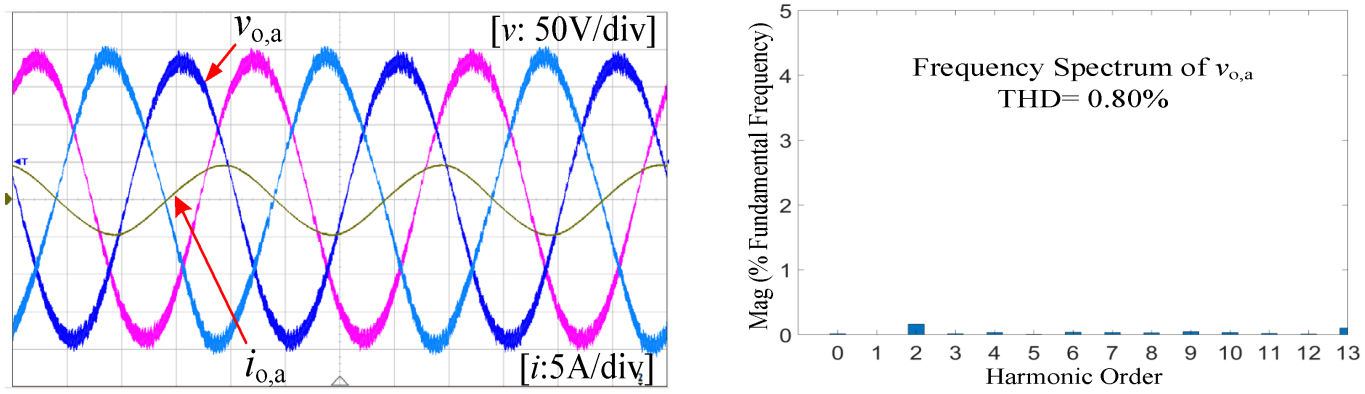
Figure 4 shows that, with P_{ref} = 500 W and Q_{ref} = 1000 Var, the VSG inverter using the state-feedback plus resonant voltage controller has a PCC voltage $v_{o,a}$ THD of 1.63%, with significant 3rd-, 5th- and 7th-order harmonic distortion components.



(**a**) (**b**)

Figure 4. Steady-state PCC voltage response of the VSG inverter using the state-feedback plus resonant voltage controller. (**a**) PCC voltages $v_{o,j}$, where j = a, b, and c, and current $i_{o,a}$; (**b**) Frequency spectrum of $v_{o,a}$.

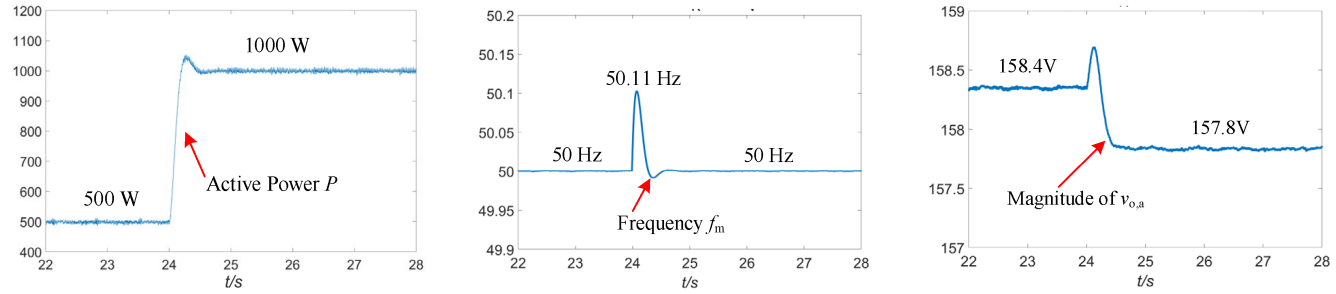
Figure 5 shows that, with P_{ref} = 500 W and Q_{ref} = 1000 Var, the VSG inverter using the proposed plug-in FARC voltage controller, i.e., the state-feedback plus the FARC controller, has a reduced PCC voltage $v_{o,a}$ THD of 0.80%, with all harmonic components almost removed by the FARC controller, as expected.



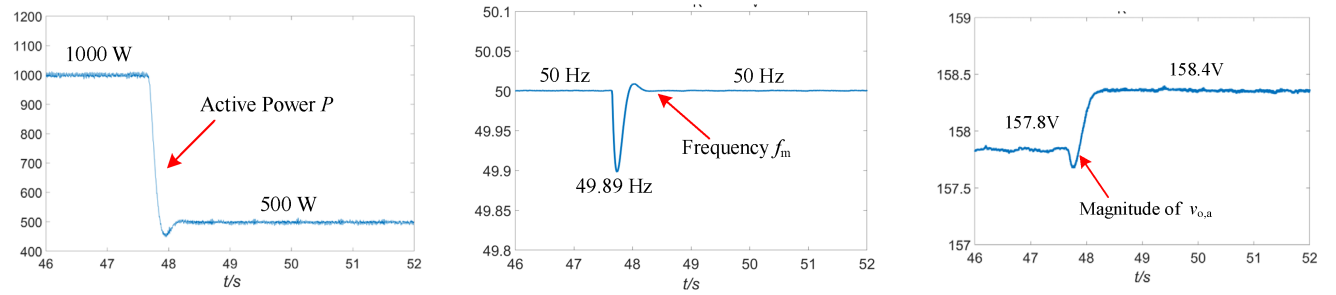
(**a**) (**b**)

Figure 5. Steady-state PCC voltage response of the VSG inverter using the proposed plug-in FARC voltage controller. (**a**) PCC voltages $v_{o,j}$, where j = a, b, and c, and current $i_{o,a}$; (**b**) Frequency spectrum of $v_{o,a}$.

Figure 6 shows the system responses of the VSG inverter using the proposed plug-in FARC voltage controller with Q_{ref} = 0 Var and step changes of P_{ref} between 500 W and 1000 W. The experimental results indicate that, without harmonic perturbations, the VSG inverter provides the primary frequency response P–ω_m specified in (1). The output active power P takes about 0.3 s to exactly track P_{ref}. Step changes of ΔP_{ref} = +/−500 W lead to a transient frequency variation of Δf_m = +/−0.11 Hz, and a slight PCC voltage change of $\Delta v_{o,a}$ = −/+0.6 V, with the PCC voltage varying between 157.8 V and 158.4 V.



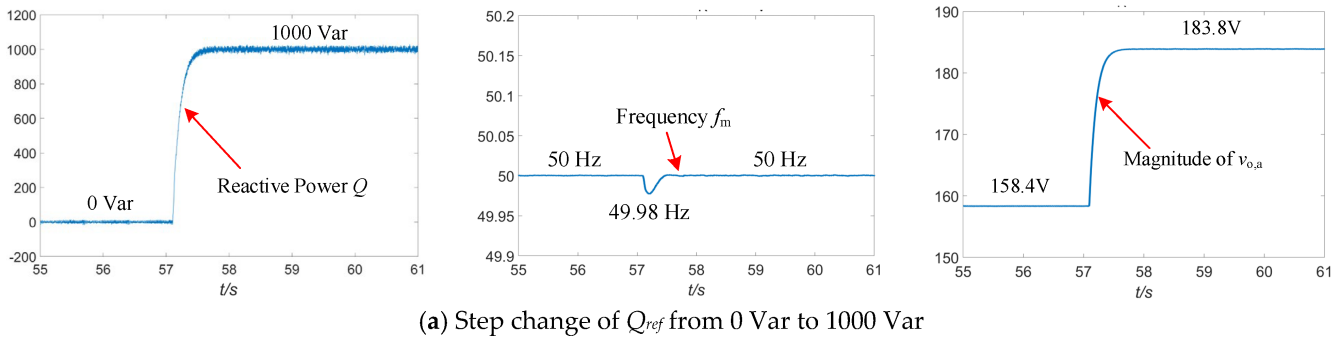
(**a**) Step change of P_{ref} from 500 W to 1000 W



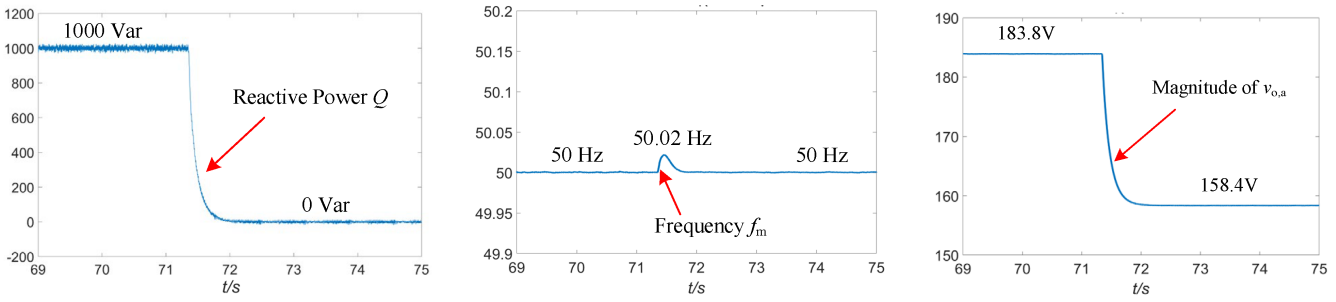
(**b**) Step change of P_{ref} from 1000 W to 500 W

Figure 6. System responses of the VSG inverter using the proposed plug-in FARC voltage controller with Q_{ref} = 0 Var and step changes of P_{ref} between 500 W and 1000 W.

Figure 7 shows the system responses of the VSG inverter using the proposed plug-in FARC voltage controller with P_{ref} = 500 W and step changes of Q_{ref} between 0 Var and 1000 Var. The experimental results indicate that, without harmonic perturbations, the VSG inverter provides the droop response $Q_{ref}-v_m$ specified in (2). The output reactive power Q takes about 0.3 s to exactly track Q_{ref}. Step changes of ΔQ_{ref} = +/−1000 Var lead to a significant PCC voltage change of $\Delta v_{o,a}$ = +/−25.4 V, with the PCC voltage varying between 158.4 V and 183.8 V, and a slight transient frequency variation of Δf_m = −/+0.02 Hz.



(**a**) Step change of Q_{ref} from 0 Var to 1000 Var



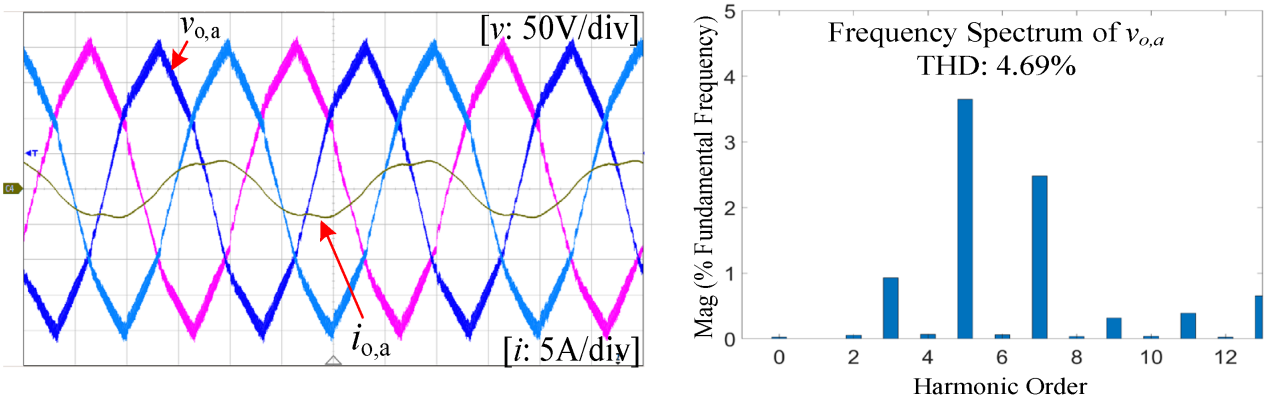
(**b**) Step change of Q_{ref} from 1000 Var to 0 Var

Figure 7. System responses of the VSG inverter using the proposed plug-in FARC voltage controller with P_{ref} = 500 W and step changes of Q_{ref} between 0 Var and 1000 Var.

3.2. System Responses Under Harmonic Perturbations

In this case, third- and fifth-order harmonic perturbations, each with a magnitude of 5% of the fundamental frequency, are injected into the grid voltages $v_{g,j}$, where $j = a$, b, and c. A rectifier load is connected to the PCC with L_L = 1 mH, C_L = 1000 µF and R_L = 150 Ω, and grid frequency f = 50 Hz.

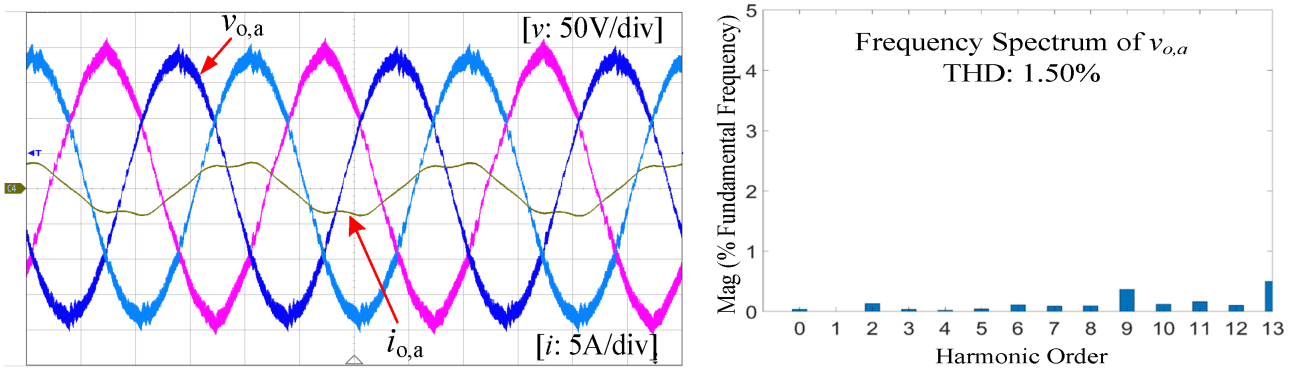
Figure 8 shows that, with P_{ref} = 500 W and Q_{ref} = 1000 Var, the VSG inverter using the state-feedback plus resonant voltage controller has a PCC voltage $v_{o,a}$ THD of 4.69% under the given harmonic perturbations, with significant 3rd-, 5th-, 7th- and higher-order odd harmonic components.



(**a**) (**b**)

Figure 8. Steady-state PCC voltage response of the VSG inverter only using the state-feedback plus resonant voltage controller under harmonic perturbations. (**a**) PCC voltages $v_{o,j}$, where $j = a$, b, and c, and current $i_{o,a}$; (**b**) Frequency spectrum of $v_{o,a}$.

Figure 9 shows that, with P_{ref} = 500 W and Q_{ref} = 1000 Var, the VSG inverter using the proposed plug-in FARC voltage controller has a PCC voltage $v_{o,a}$ THD of 1.50% under the given harmonic perturbations, with all harmonic components significantly reduced by the FARC controller, as expected.

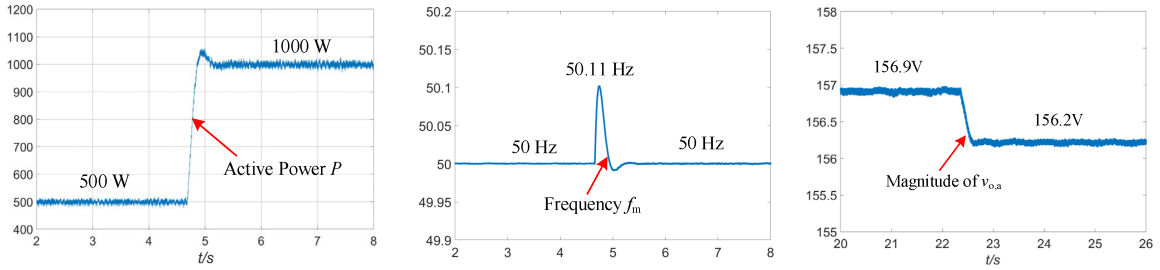


(**a**) (**b**)

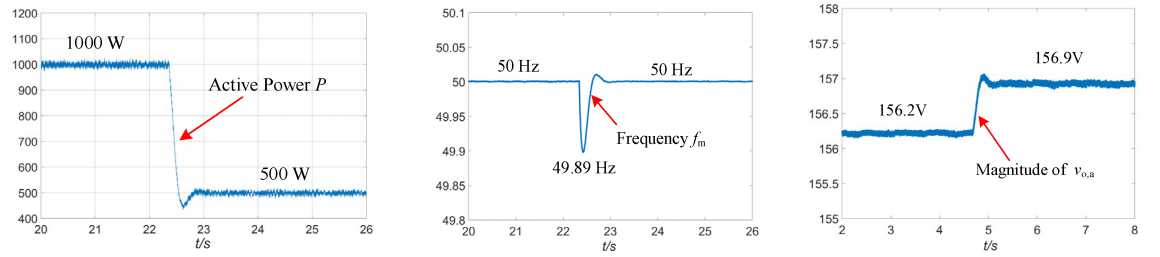
Figure 9. Steady-state PCC voltage response of the VSG inverter using the proposed plug-in FARC voltage controller under harmonic perturbations. PCC voltages $v_{o,j}$, where $j = a$, b, and c, and current $i_{o,a}$; Frequency spectrum of $v_{o,a}$.

Figure 10 shows the system responses of the VSG inverter using the proposed plug-in FARC voltage controller with Q_{ref} = 0 Var and step changes of P_{ref} between 500 W and 1000 W. The experimental results indicate that, under the given harmonic perturbations, the VSG inverter provides the primary frequency response P–ω_m specified in (1). The output

active power P takes about 0.3 s to exactly track P_{ref}. Step changes of ΔP_{ref} = +/−500 W lead to a significant frequency variation of Δf_m = +/−0.11 Hz, but only a slight PCC voltage change of $\Delta v_{o,a}$ = −/+0.7 V, with the PCC voltage varying between 156.2 V and 156.9 V.



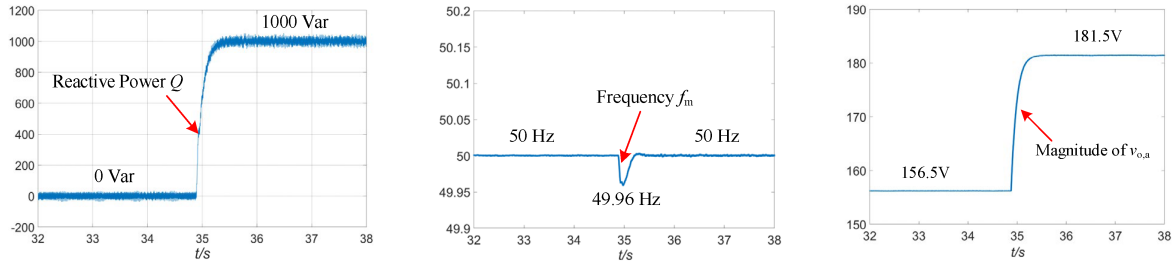
(**a**) Step change of P_{ref} from 500 W to 1000 W



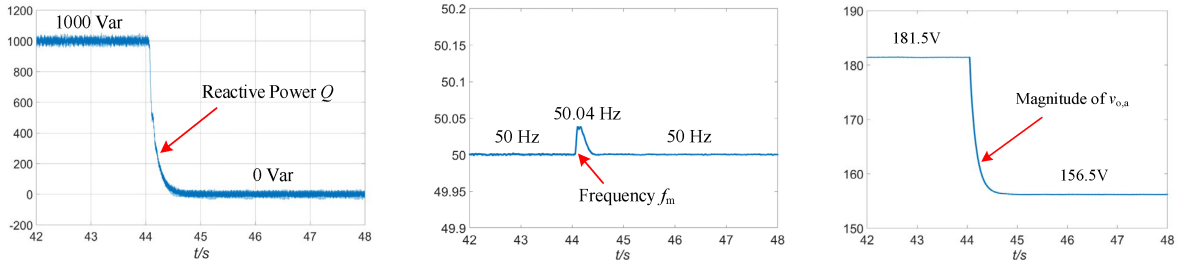
(**b**) Step change of P_{ref} from 1000 W to 500 W

Figure 10. System responses of the VSG inverter using the proposed plug-in FARC. voltage controller under harmonic perturbations with Q_{ref} = 0 Var and step changes of P_{ref} between 500 W and 1000 W.

Figure 11 shows the system responses of the VSG inverter using the proposed plug-in FARC voltage controller with P_{ref} = 500 W and step changes of Q_{ref} between 0 Var and 1000 Var. The experimental results indicate that, under harmonic perturbations, the inverter provides the droop response Q–v_m of the VSG specified in (2). The reactive power Q takes about 0.3 s to exactly track Q_{ref}. Step changes of ΔQ_{ref} = +/−1000 Var lead to a significant PCC voltage change of $\Delta v_{o,a}$ = +/−25 V, with the PCC voltage varying between 156.5 V and 181.5 V, but a small transient frequency variation of Δf_m = −/+0.04 Hz.



(**a**) Step change of Q_{ref} from 0 Var to 1000 Var



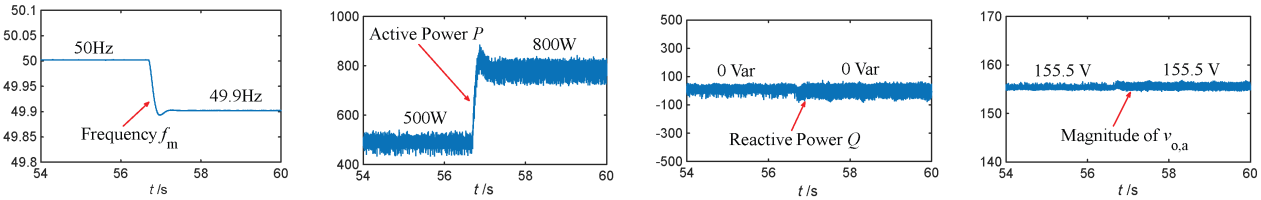
(**b**) Step change of Q_{ref} from 1000 Var to 0 Var

Figure 11. System responses of the VSG inverter using the proposed plug-in FARC voltage controller under harmonic perturbations with P_{ref} = 500 W and step changes of Q_{ref} between 0 Var and 1000 Var.

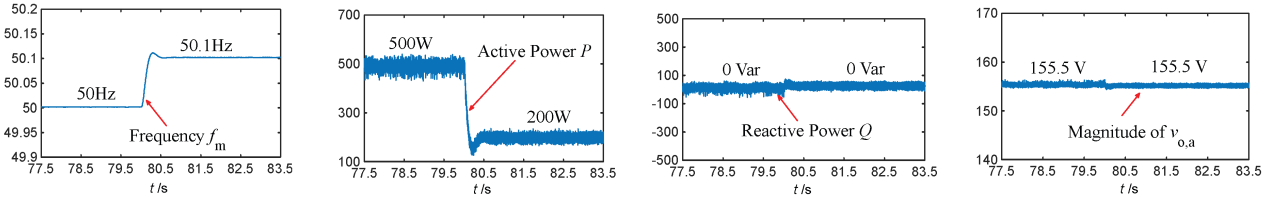
3.3. System Responses Under Grid Frequency Changes

In this case, in addition to the above-given harmonic perturbations—the nonlinear rectifier load and distorted grid voltages—the VSG inverter undergoes grid frequency changes.

Figure 12 shows the system responses of the VSG inverter using the proposed plug-in FARC voltage controller with P_{ref} = 500 W, Q_{ref} = 0 Var, and step changes of the grid frequency f. The experimental results indicate that, when f changes from 50 Hz to 49.9 Hz stepwise, the reference frequency f_m changes from 50 Hz to 49.9 Hz, and the output active power P changes from 500 W to 800 W to provide grid frequency support, while both the output reactive power Q and the magnitude of $v_{o,a}$ remain almost unchanged. When f changes from 50 Hz to 50.1 Hz, f_m changes from 50 Hz to 50.1 Hz, and P changes from 500 W to 200 W to provide grid frequency support, while both the output reactive power Q and the magnitude of $v_{o,a}$ also remain almost unchanged.



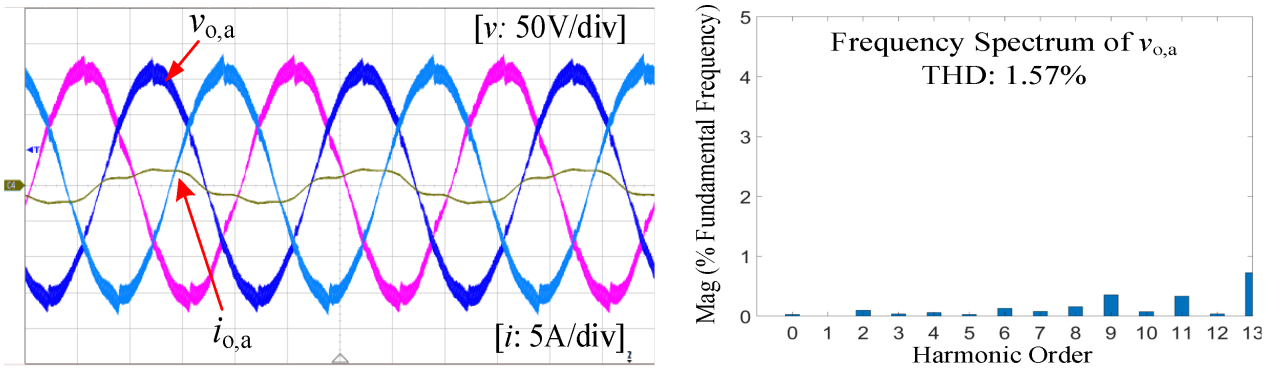
(**a**) Step change of f from 50 Hz to 49.9 Hz



(**b**) Step change of f from 50 Hz to 50.1 Hz

Figure 12. System responses of the VSG inverter using the proposed voltage controller under step changes of the grid frequency f.

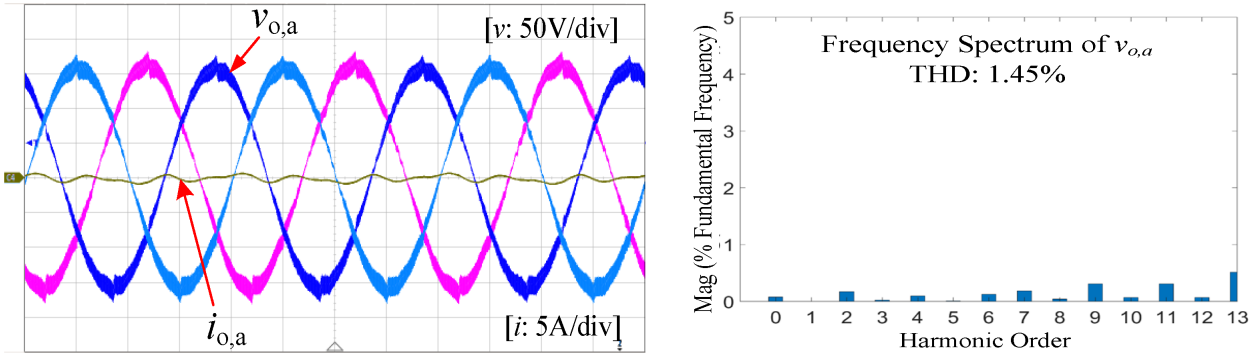
Figure 13 shows that, under $f_m = f$ = 49.9 Hz, P = 800 W, and Q = 0 Var, the VSG inverter using the proposed plug-in FARC voltage controller has a PCC voltage $v_{o,a}$ THD of 1.57%, with all harmonic components significantly reduced by the FARC controller, as expected.



(**a**) (**b**)

Figure 13. Steady-state PCC voltage response of the VSG inverter using the proposed plug-in FARC voltage controller with reference frequency $f_m = f$ = 49.9 Hz. (**a**) PCC voltages $v_{o,j}$, where $j = a$, b, and c, and current $i_{o,a}$; (**b**) Frequency spectrum of $v_{o,a}$.

Figure 14 shows that, under $f_m = f = 50.1$ Hz, $P = 200$ W, and $Q = 0$ Var, the VSG inverter using the proposed plug-in FARC voltage controller has a PCC voltage $v_{o,a}$ THD of 1.45%, with all harmonic components significantly reduced by the FARC controller, as expected.



(**a**) (**b**)

Figure 14. Steady-state PCC voltage response of the VSG inverter using the proposed plug-in FARC voltage controller with the reference frequency $f_m = f = 50.1$ Hz. (**a**) PCC voltages $v_{o,j}$ with $j = a, b, c$ and current $i_{o,a}$; (**b**) Frequency spectrum of $v_{o,a}$.

Note that the experimental results shown in Figures 4–14 are summarized in Tables 2 and 3. Generally speaking, Tables 2 and 3 show that, compared with the plug-in resonant controller, the plug-in FARC controller ensures accurate and robust compensation for various harmonic distortions and produces high-quality PCC voltages in the presence of a nonlinear rectifier load at the PCC and grid voltage distortions. Furthermore, the proposed plug-in FARC voltage control scheme enables the VSG inverter to effectively provide voltage support and frequency support—the VSG's grid-forming functionalities defined in (1) and (2)—under various harmonic perturbations and grid frequency variations.

Table 2. Steady-state PCC voltage responses using the plug-in FRAC and resonant controllers.

Item	**PCC Voltage v_{oa}**			
	Plug-in Resonant Controller		Plug-in FARC	
No load at PCC	THD = 1.63%	significant 3rd-, 5th-, 7th-order harmonics	THD = 0.8%	all harmonics are almost removed
Rectifier load at PCC	THD = 4.69%	very high 3rd, 5th, 7th harmonics	THD = 1.5%	no significant harmonics
f = 49.9 Hz under rectifier load	NA	NA	THD = 1.57%	no significant harmonics
f = 50.1 Hz under rectifier load	NA	NA	THD = 1.45%	no significant harmonics

Table 3. Dynamic system responses using the plug-in FRAC.

Step active power change with $Q_{ref} = 0$ Var	P_{ref} = 500 W → 1 kW without perturbations	Δf_m = +0.11 Hz within 0.3 s	v_{oa} = 158.4 V → 157.8 V within 0.3 s
	P_{ref} = 1 kW → 500 W without perturbations	Δf_m = −0.11 Hz within 0.3 s	v_{oa} = 157.8 V → 158.4 V within 0.3 s
	P_{ref} = 500 W → 1 kW with perturbation	Δf_m = +0.11 Hz within 0.3 s	v_{oa} = 156.9 V → 156.2 V within 0.3 s
	P_{ref} = 1 kW → 500 W with perturbations	Δf_m = −0.11 Hz within 0.3 s	v_{oa} = 156.2 V → 156.9 V within 0.3 s

Table 3. *Cont.*

Step reactive power change with P_{ref} = 500 W	Q_{ref} = 0 Var → 100 Var without perturbation	Δf_m = −0.02 Hz within 0.3 s	v_{oa} = 158.4 V → 183.8 V within 0.3 s
	Q_{ref} = 1 kVar → 0 Var with perturbations	Δf_m = +0.02 Hz. within 0.3 s	v_{oa} = 183.8 V → 158.4 V within 0.3 s
	Q_{ref} = 0 Var → 100 Var with perturbations	Δf_m = −0.04 Hz within 0.3 s	v_{oa} = 156.5 V → 181.5 V within 0.3 s
	Q_{ref} = 1 kVar → 0 Var without perturbations	Δf_m = +0.04 Hz. within 0.3 s	v_{oa} = 156.5 V → 181.5 V within 0.3 s
Step frequency change with perturbations	f = 50 Hz → 49.9 Hz	P = 500 W → 800 W within 0.3 s	Q and v_{oa} are almost unchanged
	f = 50 Hz → 50.1 Hz	P = 500 W → 200 W within 0.3 s	Q and v_{oa} are almost unchanged

4. Conclusions

VSG-based grid-forming inverters play a vital role in enabling high penetration of renewable energy sources and power electronic devices in the power grid. A simple but effective plug-in FARC voltage control scheme is proposed for the VSG control scheme to ensure good-quality PCC voltage in the presence of grid frequency variations and various harmonic perturbations—nonlinear rectifier loads, grid voltage distortions, etc. The proposed voltage controller integrates the FARC controller into the state-feedback voltage control loop. The plug-in design preserves the VSG's inherent grid-forming capabilities while avoiding control-loop redesign. A simple and efficient design and tuning method for the proposed voltage controller is provided. Experimental results indicate that the proposed voltage control strategy not only can achieve fast, accurate, and robust PCC voltage regulation to provide VSG's grid-forming functionalities—voltage support and grid frequency support—but also guarantees accurate elimination of harmonic distortions under nonlinear rectifier loads, grid voltage distortions, and grid frequency variations. The proposed strategy can be applied to both grid-following and grid-forming converters for harmonic pollution mitigation [24–27].

Author Contributions: Conceptualization, P.X. and K.Z.; methodology, K.Z.; software, J.T.; validation, L.L. and Y.S.; formal analysis, J.T.; investigation, L.L. and Y.S.; resources, P.X.; data curation, J.T.; writing—original draft preparation, P.X. and J.T.; writing—review and editing, K.Z.; visualization, L.L.; supervision, K.Z.; project administration, P.X.; funding acquisition, P.X. and K.Z. All authors have read and agreed to the published version of the manuscript.

Funding: This research was supported by State Grid Hubei Electric Power Co. Ltd. Science and Technology under Grant No. 52153224002H.

Data Availability Statement: The original contributions presented in this study are included in the article; further inquiries can be directed to the corresponding author.

Conflicts of Interest: Authors Ping Xiong, Lie Li, and Yu Sun were employed by the company State Grid Hubei Electric Power Research Institute. The remaining authors declare that the research was conducted in the absence of any commercial or financial relationships that could be construed as a potential conflict of interest. The authors declare that this study received funding from State Grid Hubei Electric Power Co. Ltd. Science and Technology under Grant No. 52153224002H. The funder was not involved in the study design, collection, analysis, interpretation of data, the writing of this article, or the decision to submit it for publication.

References

1. Markovic, U.; Stanojev, O.; Aristidou, P.; Vrettos, E.; Callaway, D.; Hug, G. Understanding small signal stability of low-inertia systems. *IEEE Trans. Power Syst.* **2021**, *36*, 1997–4017. [CrossRef]
2. Alipoor, J.; Miura, Y.; Ise, T. Power system stabilization using virtual synchronous generator with alternating moment of inertia. *IEEE J. Emerg. Sel. Top. Power Electron.* **2015**, *3*, 451–458. [CrossRef]
3. Zhong, Q.C.; Weiss, G. Synchronverters: Inverters that mimic synchronous generators. *IEEE Trans. Ind. Electron.* **2010**, *58*, 1259–1267. [CrossRef]
4. Lasseter, R.H.; Chen, Z.; Pattabiraman, D. Grid-forming inverters: A critical asset for the power grid. *IEEE J. Emerg. Sel. Top. Power Electron.* **2020**, *8*, 925–935. [CrossRef]
5. Wang, J.; Ma, K. Inertia and grid impedance emulation of power grid for stability test of grid-forming converter. *IEEE Trans. Power Electron.* **2023**, *38*, 2469–2480. [CrossRef]
6. Li, M.; Huang, W.; Tai, N.; Yang, L.; Duan, D.; Ma, Z. A dual-adaptivity inertia control strategy for virtual synchronous generator. *IEEE Trans. Power Syst.* **2019**, *35*, 594–604. [CrossRef]
7. Xu, C.; Zou, Z.; Yang, J.; Wang, Z.; Chen, W.; Buticchi, G. Transient stability analysis and enhancement of grid-forming and grid-following converters. *IEEE J. Emerg. Sel. Top. Power Electron.* **2024**, *5*, 1396–1408. [CrossRef]
8. Meng, X.; Liu, J.; Liu, Z. A Generalized droop control for grid-supporting inverter based on comparison between traditional droop control and virtual synchronous generator control. *IEEE Trans. Power Electron.* **2019**, *34*, 5416–5438. [CrossRef]
9. Rathnayake, D.B.; Razzaghi, R.; Bahrani, B. Generalized virtual synchronous generator control design for renewable power systems. *IEEE Trans. Sust. Energy* **2022**, *13*, 1021–1036. [CrossRef]
10. Deng, H.; Fang, J.; Qi, Y.; Tang, Y.; Debusschere, V. A generic voltage control for grid-forming converters with improved power loop dynamics. *IEEE Trans. Ind. Electron.* **2023**, *70*, 3933–3943. [CrossRef]
11. Wu, H.; Wang, X. Control of grid-forming VSCs: A perspective of adaptive fast/slow internal voltage source. *IEEE Trans. Power Electron.* **2023**, *38*, 10151–10169. [CrossRef]
12. Pan, D.; Wang, X.; Liu, F.; Shi, R. Transient stability of voltage-source converters with grid-forming control: A design-oriented study. *IEEE J. Emerg. Sel. Top. Power Electron.* **2020**, *8*, 1019–1033. [CrossRef]
13. Chen, M.; Zhou, D.; Blaabjerg, F. Multivariable grid-forming converters with direct states control. *IEEE Trans. Ind. Appl.* **2023**, *59*, 4334–4341. [CrossRef]
14. Chen, M.; Zhou, D.; Tayyebi, A.; Prieto-Araujo, E.; Dörfler, F.; Blaabjerg, F. Generalized multivariable grid-forming control design for power converters. *IEEE Trans. Smart Grid* **2022**, *13*, 2873–2885. [CrossRef]
15. Lou, G.; Yang, Q.; Gu, W.; Quan, X.; Guerrero, J.M.; Li, S. Analysis and Design of Hybrid Harmonic Suppression Scheme for VSG Considering Nonlinear Loads and Distorted Grid. *IEEE Trans. Energy Convers.* **2021**, *36*, 3096–3106.
16. Francis, B.A.; Wonham, W.M. The internal model principle of control theory. *Automatica* **1976**, *12*, 457–465. [CrossRef]
17. Behera, S.K.; Panda, A.K.; Naik N., V.R.; Behera, S. A Seamless enhancing grid stiffness control strategy for harmonic compensation and power ripple mitigation in grid-tied virtual synchronous generator system. *IEEE Trans. Ind. Inform.* **2025**, *21*, 6090–6101. [CrossRef]
18. Zhou, L.; Chen, Y.; Shuai, Z.; Wu, W.; Zhou, X.; Yan, K.; Luo, A. Impedance-based harmonic current suppression method for VSG connected to distorted grid. *IEEE Trans. Ind. Electron.* **2020**, *67*, 5490–5502. [CrossRef]
19. Li, S.; Wu, L.; Agundis-Tinajero, G.D.; Chaudhary, S.K.; Vasquez, J.C.; Guerrero, J.M. A decomposed harmonic current suppression method for VSG-based microgrids connected to distorted grids. *IEEE Trans. Ind. Electron.* **2024**, *71*, 10669–10680. [CrossRef]
20. Tang, C.; Zhou, K.; Shu, Y.; He, Q.; Chen, Q. Analysis and design of multiple resonant current control for grid-connected converters. *IEEE J. Emerg. Sel. Top. Power Electron.* **2022**, *10*, 2539–2546. [CrossRef]
21. Zhou, K.; Tang, C.; Chen, Y.; Zhang, B.; Lu, W. A generic multi-frequency repetitive control scheme for power converters. *IEEE Trans. Ind. Electron.* **2023**, *70*, 12680–12688. [CrossRef]
22. Zou, Z.; Zhou, K.; Wang, Z.; Cheng, M. Frequency adaptive fractional order repetitive control of shunt active power filters. *IEEE Trans. Ind. Electron.* **2015**, *62*, 1659–1668. [CrossRef]
23. Yang, Y.; Zhou, K.; Wang, H.; Blaabjerg, F.; Wang, D.; Zhang, B. Frequency adaptive selective harmonic control for grid-connected inverters. *IEEE Trans. Power Electron.* **2015**, *30*, 3912–3924. [CrossRef]
24. Liu, Y.; Wang, Y.; Wang, M.; Xu, Z.; Peng, Y.; Li, M. Coordinated VSG control of photovoltaic/battery system for maximum power output and grid supporting. *IEEE J. Emerg. Sel. Top. Circ. Syst.* **2022**, *12*, 301–309. [CrossRef]
25. Li, C.; Yang, Y.; Cao, Y.; Wang, L.; Blaabjerg, F. Frequency and voltage stability analysis of grid-forming virtual synchronous generator attached to weak grid. *IEEE J. Emerg. Sel. Top. Power Electron.* **2022**, *10*, 2662–2671. [CrossRef]

26. Dong, S.; Chen, Y.C. A method to directly compute synchronverter parameters for desired dynamic response. *IEEE Trans. Energy Convers.* **2018**, *33*, 814–825. [CrossRef]
27. Albalawi, H.; Wadood, A.; Khan, S.; Alatwi, A.K. Harmonic mitigation in multi-pulse rectification: A comparative study of 12-, 18-, and 24-pulse systems. *Mathematics* **2024**, *12*, 3257. [CrossRef]

Disclaimer/Publisher's Note: The statements, opinions and data contained in all publications are solely those of the individual author(s) and contributor(s) and not of MDPI and/or the editor(s). MDPI and/or the editor(s) disclaim responsibility for any injury to people or property resulting from any ideas, methods, instructions or products referred to in the content.